AGU PUBLICATIONS

JGR

Journal of Geophysical Research: Solid Earth

RESEARCH ARTICLE
10.1002/2014JB011713

Key Points:
- Upper lithospheric mantle is devoid of significant electrical isotropy
- MT responses are associated with large-scale resistive Archean lithosphere
- Possible dextral shearing is not associated with shape referred orientation

Correspondence to:
A. Q. Adetunji,
Ademola.Adetunji@umanitoba.ca

Citation:
Adetunji, A. Q., I. J. Ferguson, and A. G. Jones (2015), Reexamination of magnetotelluric responses and electrical anisotropy of the lithospheric mantle in the Grenville Province, Canada, *J. Geophys. Res. Solid Earth*, *120*, doi:10.1002/2014JB011713.

Received 21 OCT 2014
Accepted 3 FEB 2015
Accepted article online 7 FEB 2015

Reexamination of magnetotelluric responses and electrical anisotropy of the lithospheric mantle in the Grenville Province, Canada

Ademola Q. Adetunji[1], Ian J. Ferguson[1], and Alan G. Jones[2]

[1]Department of Geological Sciences, University of Manitoba, Winnipeg, Manitoba, Canada, [2]Geophysics Section, School of Cosmic Physics, Dublin Institute of Advanced Studies, Dublin, Ireland

Abstract Magnetotelluric (MT) responses at the Proterozoic Grenville Front in Canada have been interpreted as being caused by lithospheric electrical anisotropy, and the area is often noted as a classic example of lithospheric anisotropy. This study reevaluates evidence for the electrical anisotropy using 56 MT stations. The spatially uniform MT responses noted at the Grenville Front extend to ~200 km southeast and for at least 400 km along strike and are associated with rocks at less than 150 km depth. Examination of induction arrows at longer periods shows arrows at high angle to the MT conductive direction consistent with the presence of macroscopic resistivity structures. New 2-D anisotropic inversions show that electrical anisotropy is not required to fit the MT data. The results indicate that in the resistive mantle lithosphere beneath the Grenville Front, and in conductive lithosphere in adjacent areas, the maximum horizontal resistivity anisotropy is $<$10%, much less than the factor of 15 determined in earlier 1-D studies. The results suggest that the upper lithospheric mantle in the area is devoid of significant electrical anisotropy and that the observed MT response directionality is due to large-scale resistivity structure. We interpret the spatially consistent MT responses observed at the Grenville Front as being associated with the resistive Archean lithosphere extending southeast beneath the Grenville Front. The obliquity between seismic and MT responses arises because the Superior fabric is oblique to the seismic fast direction. If dextral shearing occurred, it appears to have not caused any significant shape preferred electrical anisotropy.

1. Introduction

The magnetotelluric (MT) method is an electromagnetic geophysical method that maps spatial variation of electrical resistivity using naturally occurring time variations of the horizontal components of the electric and magnetic fields. The method can probe the Earth from a hundred meters to depths of several hundreds of kilometers [*Chave and Jones*, 2012]. The primary MT response is the complex-valued impedance tensor, but individual terms of the tensor may be examined in terms of the corresponding apparent resistivity and impedance phase, both of which give insight into underlying resistivity structure [*Vozoff*, 1991]. The phase response is the more robust estimate for sites at which the MT response is distorted galvanically by small-scale, near-surface heterogeneities [e.g., *Groom and Bailey*, 1989; *Caldwell et al*., 2004]. A second response that is often considered in MT studies is the tipper, which defines the transfer function between the vertical and horizontal components of the magnetic field. This response is often displayed graphically using induction arrows [*Vozoff*, 1991]. In this study we use MT and induction arrow responses to reexamine evidence for electrical anisotropy in the lithospheric mantle of the Grenville Front region. We seek to determine whether the azimuthal variation in the MT responses, defined by the earlier studies, is related to electrical anisotropy or to larger-scale geological structure.

MT studies of the Grenville Front, and the adjacent Superior Province and Grenville Province, in North America have provided results that have previously been interpreted in terms of electrical resistivity anisotropy recording past tectonic deformation of the mantle lithosphere [e.g., *Kurtz et al*., 1988; *Kellett et al*., 1992; *Mareschal et al*., 1995; *Ji et al*., 1996]. The interpretation of electrical anisotropy at the Grenville Front was based on an absence of spatially consistent responses in shorter period ($<$100 s) induction arrows and on spatial uniformity of the MT responses [*Kellett et al*., 1992; *Mareschal et al*., 1995; *Boerner et al*., 2000]. *Mareschal et al*. [1995] constrained the resistivity anisotropy in this region to lie between 50 and 150 km

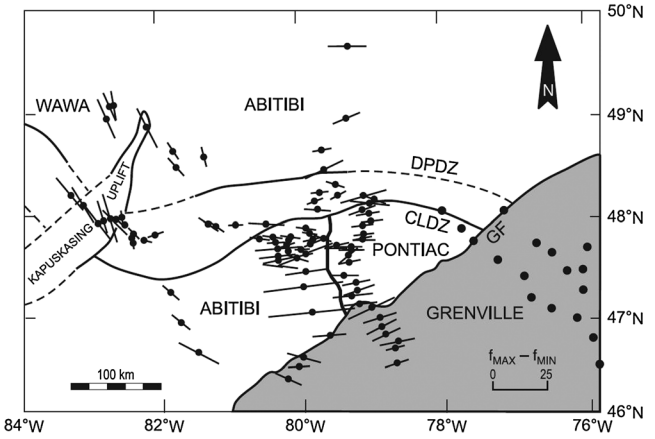

Figure 1. MT response anisotropy in the southern subprovinces of the Superior Province (Wawa, Abitibi, and Pontiac subprovinces) and the northern Grenville Province [*Boerner et al*., 2000]. DPDZ = Destor-Porcupine deformation zone; CLDZ = Cadillac-Larder deformation zone; GF = Grenville Front. The length of the line at each MT site is proportional to the phase difference between the off-principal MT impedances, and the direction is the direction of maximum phase. Sites with erratic apparent resistivity and phase responses as a function of azimuth are shown as dots.

depth with a maximum ratio of horizontal resistivities within the anisotropic layer of 1:15 and a conductive direction azimuth of N80°E (Figure 1). The authors suggested that the anisotropy may be due to the concentration of graphite in mantle shear zones correlating with observed crustal sutures. Shear wave splitting studies by *Sénéchal et al*. [1996] in the same region revealed spatially consistent seismic anisotropy with a fast direction of N103°E. Obliquity of the resistivity anisotropy and seismic anisotropy in the region led to the interpretation, now internationally renowned [e.g., *Wannamaker*, 2005], that the resistivity anisotropy in the mantle lithosphere is caused by shape alignment of the mantle minerals whereas the seismic anisotropy is caused by the crystallographic alignment [*Ji et al*., 1996; *Sénéchal et al*., 1996]. Taken together, the results implied dextral shearing in a mantle transcurrent shear zone which is consistent with the inferred motion from crustal shear zones [*Ji et al*., 1996].

Frederiksen et al. [2006] examined the directional dependence of seismic and MT responses at a larger scale across the Grenville Front. Although both seismic and MT responses show significant directional dependence over a large area of the southern Superior and Grenville provinces, the patterns observed at the Grenville Front are restricted to the area around the Grenville Front itself. The authors conclude that their analyses were unable to provide a definitive answer as to whether the MT directionality at the Grenville Front could be attributed to electrical anisotropy alone. More recently, *Adetunji et al*. [2014, 2015] show that the MT responses in the Grenville Front area can be accurately modeled by two-dimensional (2-D) models without any anisotropy. As with the earlier results, these 2-D models indicate the presence of resistive mantle lithosphere between 50 km and 150 km depth in the Grenville Province.

In the present study, broadband MT responses from a total of 56 sites are analyzed (Figure 2): these include 35 sites from the Lithoprobe Abitibi-Grenville Transect [*Boerner et al*., 2000] and 21 sites from the POLARIS (Portable Observatories for Lithosphere Analysis and Research Investigating Seismicity) project [*Eaton et al*., 2005]. The MT sites form three profiles with northwest-southeast azimuths and span a north-south distance of 500 km and an east-west distance of 650 km. The data at sites along profiles 1 and 3 have both MT and tipper responses available, but those on profile 2 have only MT responses. The MT data from profile 1 have been examined previously by *Kellett et al*. [1992], [1994], *Zhang et al*. [1995], *Mareschal et al*. [1995], *Ji et al*. [1996], *Sénéchal et al*. [1996], and *Adetunji et al*. [2014, 2015]. *Mareschal et al*. [1995], *Boerner et al*. [2000], and *Frederiksen et al*. [2006] examine the MT response anisotropy for sites in all three profiles.

The present analysis commences with a detailed depth-based study of the dimensionality of the MT response and examination of the tipper response along the three profiles in order to define the lateral and depth extent of the MT response anisotropy noted at the Grenville Front [e.g., *Mareschal et al*., 1995]. The interpretation of these results is enhanced by the availability of isotropic 2-D inversion models from the MT data in each of the three profiles determined in earlier studies [*Adetunji*, 2014; *Adetunji et al*., 2014, 2015]. This information enables the dimensionality results to be tied to a particular region of the resistivity model and assists in the tectonic interpretation of the results. MT responses from profile 1 are then used in an anisotropic inversion study in order to provide a quantitative assessment of the lithospheric electrical anisotropy in the Grenville province.

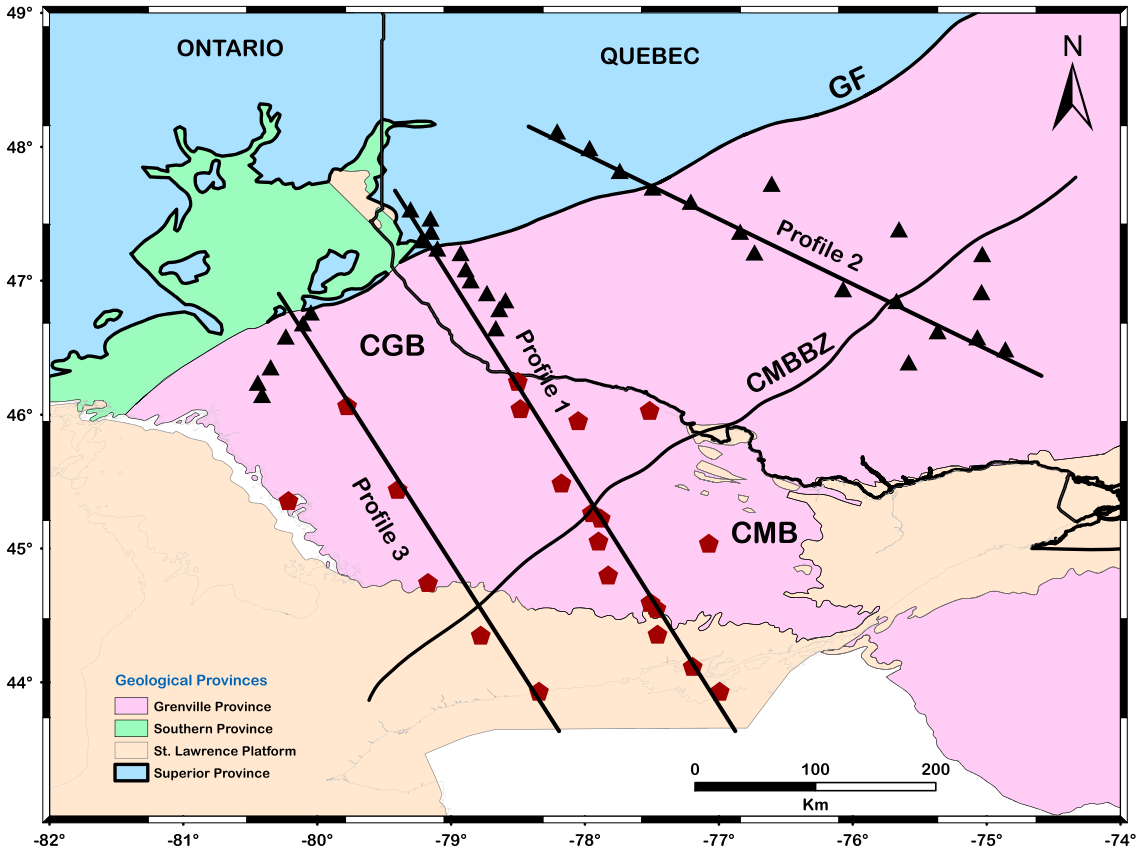

Figure 2. Map of the study area showing the locations of MT sites considered in the present study. The black triangles indicate MT sites from the Lithoprobe Abitibi-Grenville transect, and the wine-colored diamonds indicate POLARIS MT sites. Profile 1 forms part of the data analyzed by *Adetunji et al.* [2014]. The tectonic elements include the Grenville Front (GF), Central Gneiss belt (CGB), Central Metasedimentary Belt (CMB), and Central Metasedimentary Belt Boundary Zone (CMBBZ).

2. Electrical Anisotropy and MT Response Anisotropy

Electrical anisotropy, sometimes called inherent anisotropy, is the variation of the electrical conductivity (or its inverse, resistivity) as a function of direction. At the smallest scale, anisotropy is caused by alignment of minerals with different resistivities along the crystallographic axes, where it is called microscopic intracrystalline anisotropy [*Wannamaker*, 2005; *Martí*, 2014]. At larger scales, the anisotropy is called macroscopic anisotropy and arises from the superposition of individual components (ranging in size from grains to rocks to rock units) with different resistivity. All structures that produce directionality in the bulk electrical resistivity, but are too small to be resolved by the electromagnetic (EM) method being used, are usually considered to constitute electrical anisotropy. In order for electrical anisotropy to occur, the more conducting phases must be at least partially interconnected over a distance of the order of the inductive scale length [*Everett*, 2005]. For the MT method, the resolution of an MT survey is limited predominantly by the diffusive nature of induced EM propagation and also by the geometric nature of the galvanic response to charges on lateral conductivity gradients. The inductive scale length is usually on the order of hundreds of meters to kilometers [*Vozoff*, 1991], so the sources of macroanistropy may be quite large. In the lithospheric mantle, features of up to tens of kilometers could contribute to macroscopic anisotropy.

Hydrogen diffusion in mantle minerals, such as olivine or minerals with similar crystal alignment, has been identified as an important cause of electrical anisotropy in the mantle [*Schock et al.*, 1989; *Karato*, 1990; *Mackwell and Kohlstedt*, 1990; *Ji et al.*, 1996; *Hirth et al.*, 2000; *Wannamaker*, 2005; *Pommier*, 2014]. Olivine is mildly electrically anisotropic when dry [*Du Frane et al.*, 2005], but significantly more so when wet [e.g., *Poe et al.*, 2010], and is the most abundant mineral in the upper mantle. Its crystals align preferentially when under strain, and thus, many crystals with similar alignment would contribute to the overall anisotropic effect. *Jones* [1992]

suggested that the anisotropy in the mantle could also be caused by preferred interconnection of graphite minerals along a foliation in the uppermost mantle.

The MT tensor defines the surface electromagnetic impedance corresponding to electric current flow in different horizontal directions. The MT response may be directionally dependent. For example, in the MT response of 2-D structures, the phase and apparent resistivity of the transverse electric (TE) mode (corresponding to currents flowing parallel to the strike) will generally differ from those of transverse magnetic (TM) mode (corresponding to currents flowing perpendicular to the strike). This directionality is also sometimes loosely called anisotropy, but herein we will refer to this effect as MT response anisotropy to distinguish it from anisotropy related to the material properties. Response anisotropy will occur at MT sites in 2-D or 3-D resistivity structures or over general anisotropic structures. It will be absent only for MT sites over 1-D (horizontally layered) resistivity structures or over layered anisotropic rocks in which the projection of the anisotropic conductivity ellipsoid onto the horizontal plane gives equal conductivity in the horizontal directions [e.g., *Heise et al*., 2006]. A number of studies have examined ways of discriminating whether observed anisotropic MT responses are caused by resistivity anisotropy or by 2-D or 3-D resistivity structures. *Wannamaker* [2005] and *Martí* [2014] provide reviews of these approaches.

As discussed in *Heise et al*. [2006] a number of studies have interpreted relatively widespread consistent azimuthal MT phase splits as indicative of anisotropy in an underlying 1-D, layered, resistivity structure. This interpretation has usually been supported by observation of a lack of consistent large-scale tipper responses perpendicular to the structure [*Rasmussen*, 1988; *Kellett et al*., 1992; *Kurtz et al*., 1993; *Eisel and Bahr*, 1993; *Mareschal et al*., 1995; *Simpson and Tommasi*, 2005]. However, such interpretations must be made with care; they require that lateral conductivity variations be absent on a scale much larger than the conductivity gradient producing the phase split and verification that a smaller tipper response is not simply due to 2-D resistivity structures [*Heise et al*., 2006].

In 2-D structures the effects of anisotropy can be quite complex and depend on the resistivity structures, the distribution and form of anisotropy, the site location, and the period [e.g., *Heise and Pous*, 2001]. There are a number of effects that may be observed, including tipper responses and induction arrows that are misaligned with the 2-D structure, divergence of MT strike directions from the true strike, MT phases lying outside the usual quadrant for 2-D responses, and the appearance of unrealistic structures in 2-D resistivity models fitted to the MT data [*Pek and Verner*, 1997; *Weckmann et al*., 2003; *Heise and Pous*, 2001, 2003; *Wannamaker*, 2005; *Martí*, 2014]. In general, these effects can also be modeled in terms of 3-D structures [*Nieuwenhuis et al*., 2013], although in some cases a 2-D anisotropic model provides a more geologically reasonable explanation [e.g., *Baba et al*., 2006; *Le Pape et al*., 2012]. Discriminating the presence of anisotropy in 3-D resistivity structures is even more complex [*Wannamaker*, 2005; *Martí*, 2014]. *Weidelt* [1999] showed that the response from any 3-D model containing anisotropy can equivalently be explained by a 3-D isotropic model of arbitrary complexity [*Wannamaker*, 2005].

3. Tectonic Overview

The Grenville Province was formed between 1090 and 980 Ma as a result of the Himalayan-scale Grenville orogeny [*Rivers et al*., 2012]. This orogeny produced a northwest trending (present-day coordinates) thrusting of a composite belt of continental crust and magmatic rocks onto the margin of the Laurentian craton [*Carr et al*., 2000], creating a collage of tectonically stacked domains separated by ductile shear zones [*Davidson et al*., 1982; *Culshaw et al*., 1983; *Rivers et al*., 1989]. The accepted orogenic model incorporates pre-Grenvillian continental-margin arc magmatism and accretionary tectonics followed by repeated episodes of continental collision that resulted in crustal thickening, followed by orogenic collapse and emplacement of mantle- and lower crustal-derived magmas [*Rivers*, 1997; *Rivers et al*., 2012]. The final stage of the convergence at 1000 Ma affected the Grenville Front Tectonic Zone along the length of the orogen [*Haggart et al*., 1993].

The tectonic subdivision of the study region includes the Laurentian margin, which is the lowest unit in the orogenic stack. This is overlain to the southeast by the Central Gneiss Belt (CGB), which is characterized by upper amphibolite- to granulite-facies metamorphic assemblages. The CGB is in turn overlain by the Central Metasedimentary Belt (CMB), which consists of several arc and/or back-arc terranes that are characterized by greenschist- to amphibolite-facies assemblages. The CMB is separated from the CGB by the Central Metasedimentary Boundary Belt Zone (CMBBZ). Shear indicators in this zone indicate thrusting

of the CMB northwestwardly against the CGB (Figure 2) [*Rivers et al.*, 1989; *Easton*, 1992; *Rivers*, 1997; *Davidson*, 1998; *Carr et al.*, 2000; *Rivers et al.*, 2012].

At the Laurentian margin, pervasive ductile fabrics and generally shallow dipping structures have been interpreted to have formed during late orogenic extension [*Culshaw et al.*, 1997]. Within the CMB, the moderately to steeply dipping brittle-ductile normal faults contrast in age and style with those observed in the northwest [*Carr et al.*, 2000; *Rivers et al.*, 2012]. The postulated Cretaceous Great Meteor hotspot trail is interpreted to have passed through the Grenville Province's lithosphere [*Crough*, 1981; *Sleep*, 1990; *Adetunji et al.*, 2014, 2015]. This mantle plume has been associated with the Mesozoic kimberlite magmatism at Cobalt and Kirkland Lake fields in southern Ontario [e.g., *Meyer et al.*, 1994; *Ji et al.*, 1996; *Griffin et al.*, 2004; *Faure et al.*, 2011; *Adetunji et al.*, 2014, 2015].

4. Depth-Transformed MT Response Anisotropy

4.1. Analysis Strategy

In this section, we characterize variation of the dimensionality and anisotropy of the MT response with location and with period, or equivalently depth. Spatial variation in the electrical resistivity affects the depth of penetration of MT responses, so a given period may correspond to different depths at different sites [e.g., *Hamilton et al.*, 2006; *Miensopust et al.*, 2011; *Adetunji et al.*, 2014, 2015]. The Niblett-Bostick approximate transformation from period to depth [*Niblett and Sayn-Wittgenstein*, 1960; *Bostick*, 1977; *Jones*, 1983] provides a superior method for comparing related responses than period-based data analyses [*Jones*, 2006; *Jones et al.*, 2014].

The dimensionality and strike determination methods applied are phase tensor analysis [*Caldwell et al.*, 2004] and Groom-Bailey (GB) tensor decomposition [*Groom and Bailey*, 1989, 1991; *McNeice and Jones*, 2001]. Both methods provide a measure of the dimensionality and directionality of the resistivity structures responsible for the MT response while allowing for galvanic distortion. They both provide a measure of the response anisotropy in terms of the estimated phase of the principal impedance tensor responses. A small phase difference indicates responses close to those of a 1-D structure, whereas a large phase difference implies significant 2-D or 3-D regional structures [*Hamilton et al.*, 2006; *Miensopust et al.*, 2011] or anisotropy within the layers of a 1-D structure [*Heise et al.*, 2006].

We characterize the MT response anisotropy in terms of the most conductive direction. For the phase-based phase tensor and GB decomposition methods this is the direction of largest impedance phase. For sites adjacent to a linear 2-D conductor the conductive direction will correspond to geoelectric strike. However, at a 2-D resistivity contrast between resistive and conductive blocks, the conductive direction will be parallel to strike in the resistive block but perpendicular to strike in the conductive block. An observed 90° flip in the conductive direction can therefore be used to identify the location of a resistivity boundary [*Hamilton et al.*, 2006; *Miensopust et al.*, 2011]. For anisotropic 1-D structures the azimuthal dependence of the phase response is caused by the resistivity contrast at the top and base of the anisotropic layer, and the most conductive direction may correspond to either the highest or lowest component of the horizontal projection of the conductivity tensor [*Heise et al.*, 2006].

4.2. Phase Tensor Results

The phase tensor method does not require any assumption regarding the dimensionality of the regional resistivity structure, and the results remain valid when both the galvanic distorting local heterogeneity and the regional structures are both 3-D [*Caldwell et al.*, 2004]. There are two negative attributes: it operates on individual frequency responses and responses have noise that is not considered in the analysis. The phase tensor skew provides a measure of the three-dimensionality of the response. *Booker* [2014] suggested that a nonzero phase tensor skew β is the appropriate measure for indicating depth variation of the structural azimuth or anisotropy. Although a large value of the skew angle implies a 3-D regional conductivity structure, a small value of the skew angle is not necessarily a good indication of the closeness of the conductivity structure to 2-D [*Caldwell et al.*, 2004]. Constancy of the direction of the principal axes of the phase tensor, with period and with location, provides a more reliable indicator of two-dimensionality [*Caldwell et al.*, 2004].

Figure 3 shows the phase tensor maps, at different depths, for sites in the study area. We use the Niblett-Bostick approximate depth transformation of the Berdichevsky (arithmetic) average of the off-diagonal elements of the impedance tensor to convert from period to depth. Results were obtained at 50 km depth

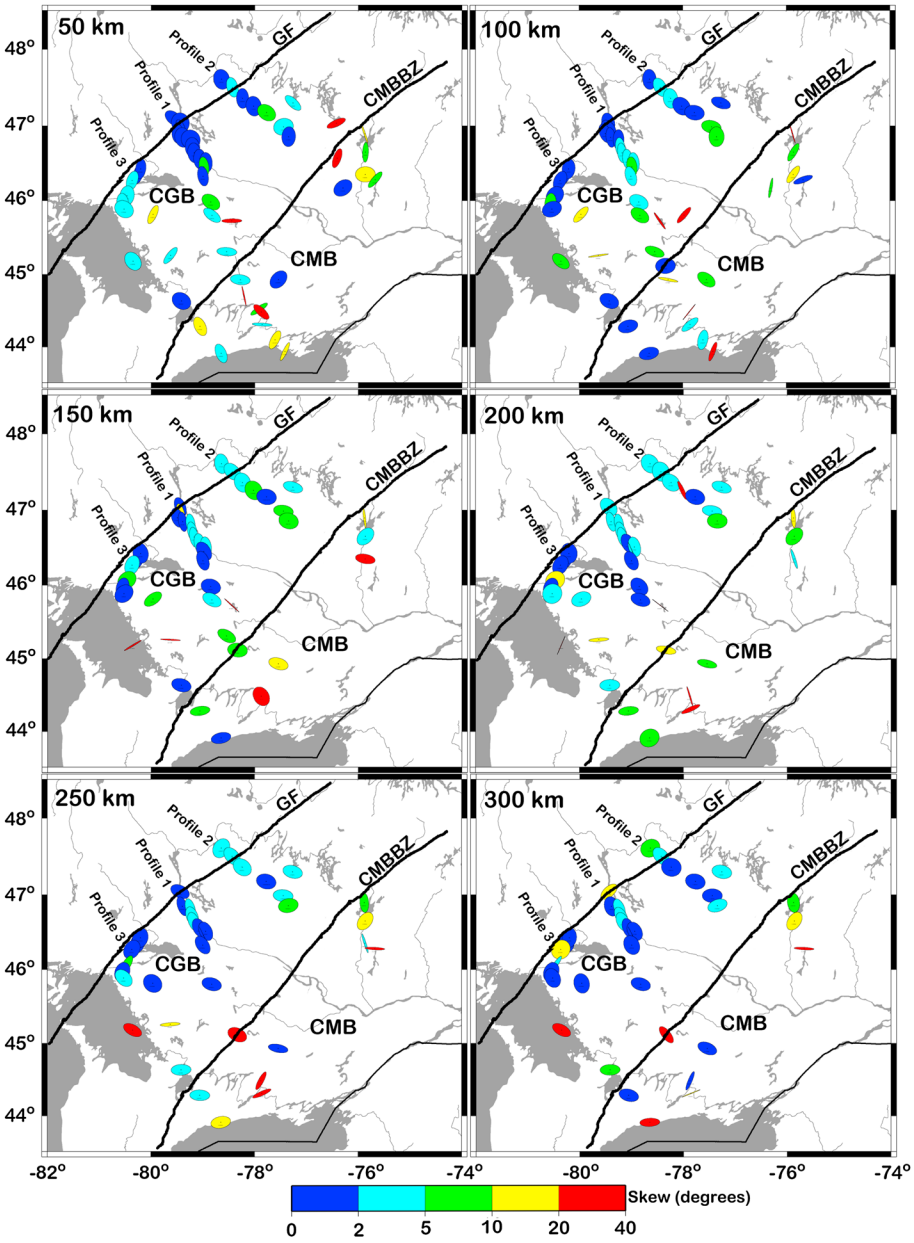

Figure 3. Phase tensor response at different Niblett-Bostick depths. The phase tensors are plotted using the MTMAP programs that plot MT parameters using Generic Mapping Tools [*Wessel and Smith*, 1991]. They are plotted with the major axis having a uniform length on the plot and the minor axis proportional to the phase of the lower phase component of the impedance. Circular symbols correspond to 1-D responses and more elliptical symbols to 2-D or 3-D responses. The phase tensor symbols are colored by the phase skew angle: blue colors correspond to 1-D and 2-D responses and yellow and red symbols to strongly 3-D responses. MT responses with large uncertainties are excluded.

increments by choosing the closest response to the specified depth. The number of sites with data that penetrate deeper than 150 km is limited, especially on profile 2 and within the CMB.

At all depths, the phase tensor skew β is relatively small ($<5°$) and there is good spatial consistency of phase ellipse orientation, for sites extending over a northwest-southeast distance of ~200 km from northwest of the Grenville Front to the middle of the CGB. These observations are consistent with the presence of 1-D or 2-D structures [*Caldwell et al.*, 2004] in this region. Within this zone, the axes of the phase tensor are mostly aligned roughly east-west or north-south on profiles 1 and 2 and WNW to ESE on profile 3.

The observed phase tensor skew and constancy of ellipse orientation indicates that responses near the Grenville Front and in the northwestern part of the CGB are dominantly 2-D. Farther to the southwest, higher values of phase skew and less uniform ellipse orientations are observed suggesting the presence of localized 3-D structures.

In the southeast part of the CGB and in the CMB, phase tensor skews are higher, and very strong phase differences are observed. The observation of strong differences in responses between some nearby sites suggests that some of the variation observed in this region is also caused by noise in the MT responses. The area is more heavily populated than areas farther to the north making the acquisition of high quality MT data quite difficult. For profile 1, at depths of less than 150 km, the directions of the principal axes of the phase tensors in this zone are somewhat aligned with azimuths between east-west and WNW-ESE. On profile 2, the alignment of the phase tensors at sites near the CMBBZ appears to be orthogonal to this structure, although a similar response is not observed on the other profiles. In contrast, for profile 3 at a depth of 50 km, phase tensor ellipses are aligned in a relatively consistent northwest-southeast direction. At depths exceeding 100 km this alignment becomes more east-west and is moderately consistent between sites.

4.3. Groom-Bailey Tensor Decomposition Results

Determination of dimensionality and the azimuth of regional response anisotropy can also be done using Groom-Bailey (GB) tensor decomposition [*Groom and Bailey*, 1989, 1991; *McNeice and Jones*, 2001]. Positive attributes of the method are that it uses all of the information in the impedance tensor and that it accommodates errors in the MT data in an appropriate statistical manner. A negative attribute is the required assumption of a regional 2-D resistivity model, although the validity of that assumption is tested statistically. Even after tensor decomposition is done to remove the effects of galvanic distortion on MT responses, the apparent resistivity may still be affected by "site gain," a static shift frequency-independent multiplicative factor operating on both apparent resistivity curves [*Jones*, 1988, 2012]. The quality of the fit of the GB model to an observed data set provides a measure of the three-dimensionality of the regional structure. A large normalized root mean square (RMS) misfit provides an indication that the data are unable to be explained by a 1-D or 2-D regional resistivity structure.

In the present study the GB decompositions were performed using the STRIKE program [*McNeice and Jones*, 2001]. *Adetunji et al.* [2015] present the results of a GB analysis for the region using depth ranges corresponding to the upper and lower mantle lithosphere, but here we present results for more narrow depth ranges. Decomposition results were obtained for individual sites using least squares fits over six ~50 km thick depth bands between 45 and 350 km. Since this study is focused on the mantle lithosphere, a depth of 45 km was chosen for the top of the shallowest depth band based on the seismically defined Moho depth for this region [*White et al.*, 2000; *Eaton et al.*, 2006]. This depth band extended from 45 to 100 km. Each of the other five bands was 50 km thick. The GB misfits were calculated using the default impedance error floor of 3.5%, which corresponds to a 7% error for the apparent resistivity and 2° for phase. This floor was calculated based on the largest impedance value and applied in an absolute manner to the other three. For these values, normalized RMS misfits exceeding 2.0 are often regarded as indicative of significantly 3-D structures [*Jones*, 2012].

Figure 4 shows the results of the GB tensor decompositions. For most of the sites, the RMS misfit of the GB model for the 50 km bands was less than 1.0. However, at isolated sites, particularly in the CMB where the phase tensor results indicated the presence of 3-D structures or of noisy data, values of up to 4.0 occur.

In regions around the Grenville Front and the northwest part of the CGB the conductive direction at depths of less than 150 km on profiles 1 and 2 has a dominantly N85°E azimuth. In contrast to the results on profiles 1 and 2, the conductive direction in the same region along profile 3 has an overall E20°S trend. Within this depth range the phase split is typically in the range of 5° to 20°. The conductive direction azimuth, at depths of less than 150 km depth in the southeast CGB and CMB, is more erratic than further to the northwest but displays more site-to-site consistency than the phase tensor results (Figure 4). The greater consistency of the GB results is explained by the greater degree of averaging in the GB analysis and the superior accommodation of noise. Although there is some dispersion, the majority of

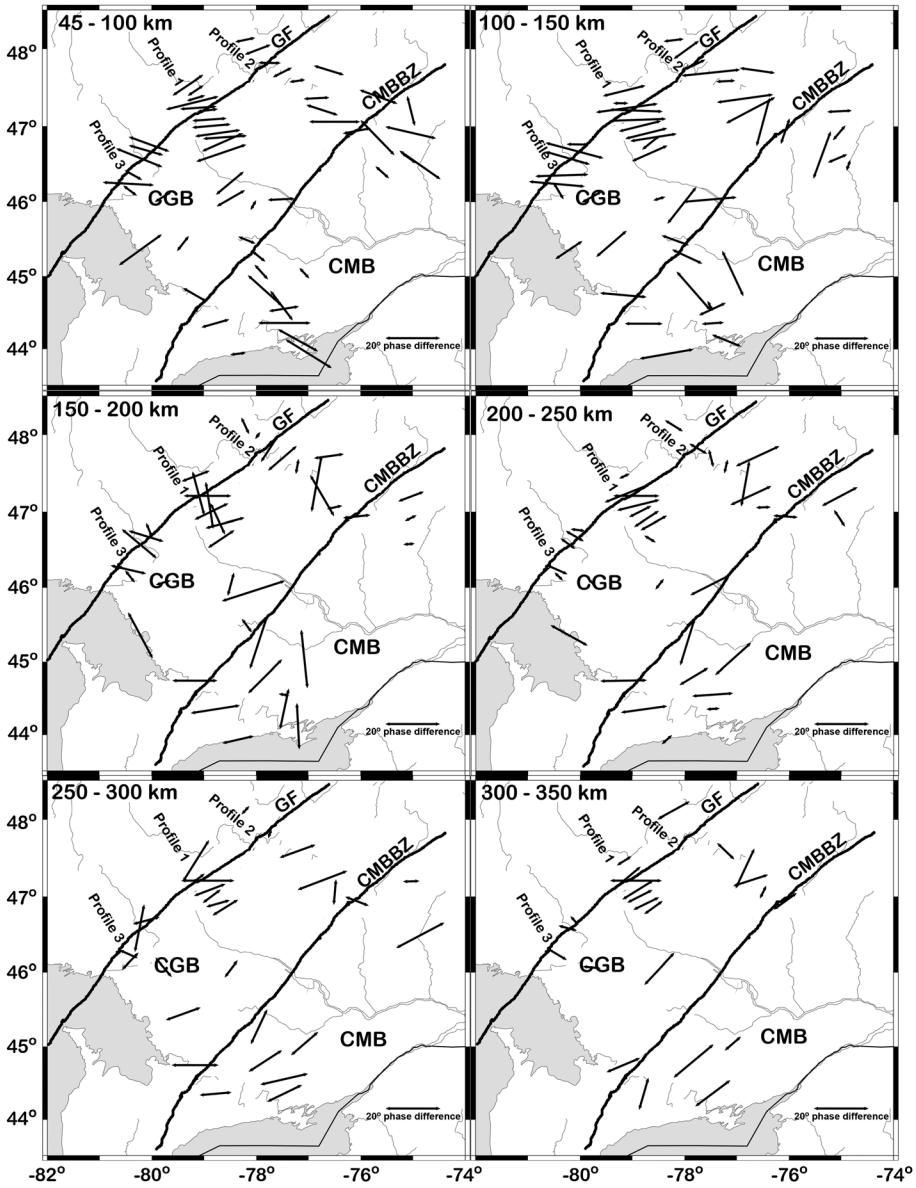

Figure 4. Results of GB strike determination for ~50 km thick depth ranges extending from 45 to 350 km. The arrows show the azimuth of the GB regional impedance with the highest phase. The length of the arrow is proportional to the average phase difference, between the maximum and minimum phase values over the depth band.

conductive directions in the CMB are parallel or perpendicular to a southwest-northeast azimuth with phase splits between 10° and 20°.

The spatial consistency of the conductive directions decreases in the 150 to 200 km depth band. On profile 1 the response near the Grenville Front and in the northwest CGB is characterized by a number of 90° flips in azimuth. This effect may be explained in part by the penetration of the Niblett-Bostick depth estimates through the base of the layer creating the 2-D response. However, there is also a transition from azimuths aligned in N80°E direction to those with a ~N65°E orientation.

At larger signal penetration (>200 km) there is a reasonable level of coherence in the conductive directions across the study area. The majority of sites show a conductive direction with a southwest to northeast azimuth and phase splits between 10° and 20°. This consistency is again far stronger than that observed in the more disparate phase tensor results (Figure 3) and attests to the superiority of the GB approach.

4.4. Review of MT Response Anisotropy

Primary observations that can be drawn from the phase tensor (Figure 3) and GB results (Figure 4) are as follows:

1. Spatially consistent conductive directions are observed at depths of <150 km from the southern Superior craton to locations in the CGB that lie within approximately 100 km southeast of the Grenville Front. On profiles 1 and 2 azimuths in this region are ~N85°E (E15°N), whereas on profile 3 they are N110°E (E20°S).
2. In the southwest CGB and CMB the conductive directions at depths of <150 km are more erratic, but the majority of sites have conductive directions parallel or perpendicular to a N45°E azimuth.
3. A transition in the responses occurs at a Niblett-Bostick depth of ~150 km. Below this depth, the east-west conductive direction observed near the Grenville Front no longer occurs. In addition, flips in the conductive direction at sites in the middle of the CGB suggest the transition across a major resistivity contrast.
4. Across the whole area, azimuths at depths exceeding 200 km are mostly parallel or perpendicular to a ~N45°E direction.

The conductive direction results can be compared with those from previous MT studies. The results for the upper 150 km of profile 1 are in agreement with the earlier studies of *Mareschal et al*. [1995] and others (Figure 1) who noted a conductive direction azimuth of N80°E and a phase split of 20° at sites within about 50 km of the Grenville Front. In contrast to the earlier studies, our results show that a similar response extends several hundred kilometers east to sites on profile 2. *Boerner et al*. [2000] noted that the MT sites on profile 2 in the northern Grenville Province exhibited erratic azimuths and magnitudes and had a different character from responses along profile 1. It is probable that this observation was influenced by galvanic distortions of the responses on profile 2 that were more effectively removed by the phase tensor and GB tensor decomposition approaches in the present study. The present results are also consistent with the period-based analysis of *Frederiksen et al*. [2006] and with analysis by *Adetunji et al*. [2015] using thicker depth ranges.

5. Induction Arrows

An important justification for the interpretation of the presence of laterally pervasive and extensive resistivity anisotropy in the vicinity of the Grenville Front was the observation of relatively small and inconsistent induction arrows across an area with very consistent MT response anisotropy [*Kellett et al*., 1992; *Mareschal et al*., 1995; *Boerner et al*., 2000]. *Kellett et al*. [1992] show an example of the data on which these interpretations were based, the induction arrows for periods of 11 s and 85 s at sites in the Pontiac subprovince on profile 1, to the north of the present study area. *Heise et al*. [2006] discussed the limitations of this interpretational method and, together with the recent results of *Adetunji et al*. [2014, 2015], who were able to fit combined MT and tipper data from profile 1 to a reasonable statistical level with isotropic 2-D models, raise uncertainty about the validity of the interpretation.

For the present study tipper data are available for sites on profiles 1 and 3 but not on profile 2, as the vertical magnetic field was not recorded at sites on this profile. As the tipper response is based on the presence of 2-D or 3-D resistivity structures, for a uniform source field [e.g., *Jones and Spratt*, 2002], it is inappropriate to use the 1-D Niblett-Bostick transform to represent these data. Also, the effects of a particular resistivity structure may be observed at quite different periods in the MT and tipper responses [e.g., *Wu et al*., 2005]. Figure 5 shows maps of the induction arrows at different periods.

The data were edited to exclude power line effects and erratic points characterized by jumps in tipper magnitudes, tipper magnitudes greatly exceeding unity, and/or large error estimates. Based on the study of *Zhang et al*. [1993], short-period (period <0.1 s) tipper data were excluded because of potential magnetic effects of galvanic distortion.

As noted in previous studies, induction arrows are relatively small in the study area. The typical length of the real induction arrows is 0.1–0.3 at 40 s period, 0.2–0.3 at 100 s period, and 0.2–0.5 for periods between 320 and 500 s. As has been previously noted, the induction arrows appear to be somewhat erratic and spatially inconsistent. However, careful examination reveals a number of large-scale spatial trends in the data particularly at longer periods.

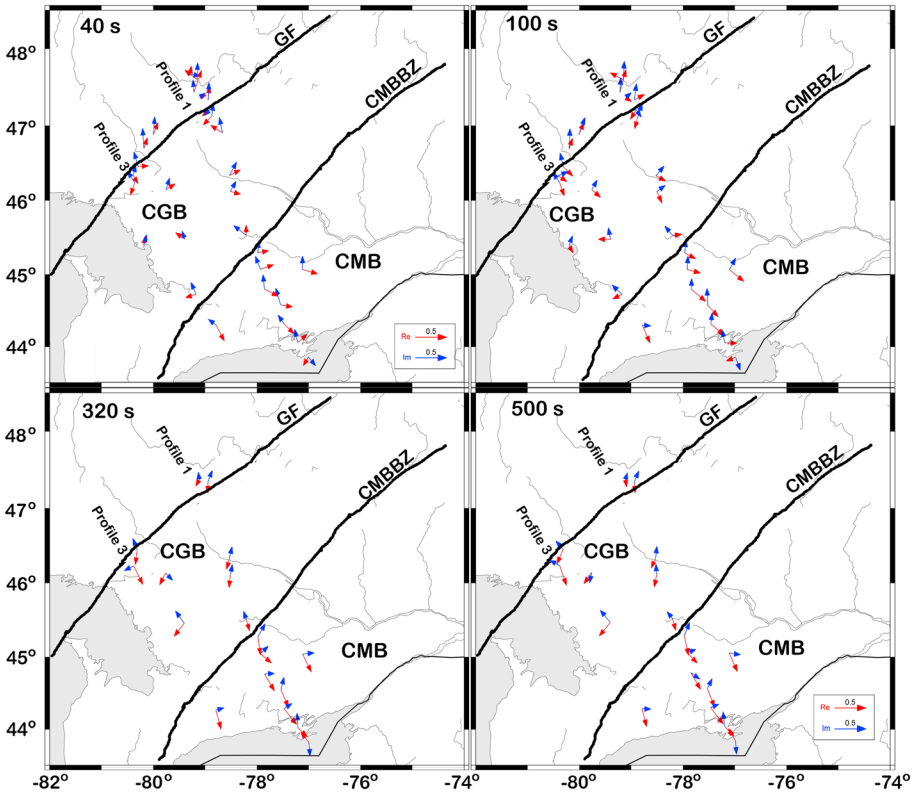

Figure 5. The induction arrow responses at 40 s, 100 s, 320 s, and 500 s, for sites along profiles 1 and 3. The real induction arrows, plotted using the *Parkinson* [1962] convention, are denoted by red arrows, and the imaginary arrows are denoted by blue arrows. Note that responses with large uncertainties are excluded.

At a period of 40 s along profile 1 and profile 2 the real induction arrows exhibit spatially variable responses (Figure 5) that are different from the upper lithospheric mantle geoelectric strike (Figure 4). *Kellett et al*. [1992] showed similar response in the Pontiac subprovince. The azimuths of the real induction arrows tend to be fairly consistent within small groups of sites over spatial scales of around 50 km or less, so it is possible that this response is influenced by local, shallow or crustal-scale structures. For example, the arrows point outward from the region of E20°S strikes and the gravity high on profile 3 south of the Grenville Front on profile 3.

The imaginary induction arrow direction at 40 s period is much more spatially consistent than the real component. At a large majority of sites on profiles 1 and 2 the imaginary arrow has a significant northward component. *Kellett et al*. [1992] showed that farther to the north, the imaginary component of the 11 s induction arrows is dominantly northward in the southern Pontiac but reverses to southward in the northern Pontiac. Examination of the theoretical tipper response of a contact between resistive and conductive quarter spaces shows at a given distance from a contact that the effects of the contact are observed at a smaller period in the imaginary response than the real response, particularly on the resistive side of the contact. The observed results are thus consistent with the presence of relatively large scale resistivity structures.

At longer periods there is a significant amount of spatial consistency in the induction arrow responses. At 320 s and 500 s the real induction arrows point mainly to the SSE (E70°S), although there is a reversal observed at the southernmost site on profile 2 at a latitude of approximately 44°N. The larger, and thus better resolved, imaginary arrows tend to point in the antiparallel direction to the corresponding real arrows, providing support for the existence of large-scale 2-D resistivity structures [e.g., *Booker*, 2014].

The reexamination of the induction arrow responses near the Grenville Front using the larger data set available in the current study leads to a revised conclusion concerning their support for anisotropic resistivity. The induction arrow responses for periods longer than 100 s provide a strong indication of the presence of large-scale 2-D (or 3-D) resistivity structures. Even at shorter periods of 10–100 s the arrows appear to

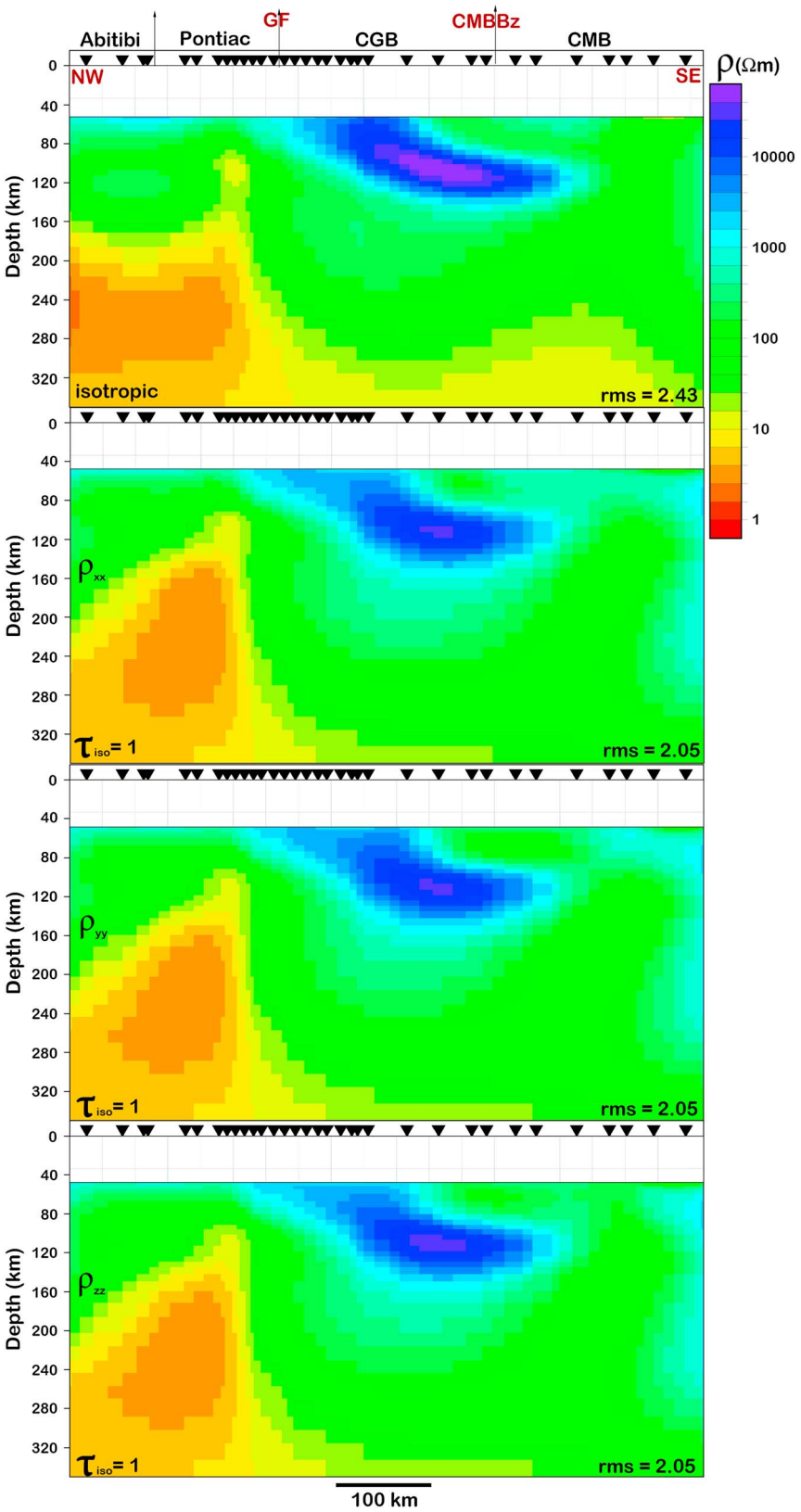

Figure 6. Isotropic and anisotropic inversion (using $\tau_{iso} = 1$) models for profile 1. The anisotropic inversion results are for the along-strike ρ_{xx}, cross-strike ρ_{yy}, and vertical ρ_{zz} components of the resistivity. The crustal section (upper 48 km) of the model is not shown.

Table 1. Summary of Parameters and Results of Isotropic and Anisotropic Inversion for Profile 1[a]

				Cross Section Through Resistor				Cross Section Through Conductor			
				ρ_{yy}/ρ_{xx}		ρ_{zz}/ρ_{xx}		ρ_{yy}/ρ_{xx}		ρ_{zz}/ρ_{xx}	
Model	τ	τ_{iso}	RMS	Mean	Median	Mean	Median	Mean	Median	Mean	Median
Isotropic	6	10^6	2.43	1.00	1.00	1.00	1.00	1.00	1.00	1.00	1.00
Anisotropic	6	1.0	2.05	1.04	1.06	1.01	1.01	1.08	1.06	1.00	0.99
Anisotropic	6	0.1	1.99	1.91	2.02	1.15	1.22	2.28	1.97	1.00	1.05
Anisotropic	6	0.01	1.96	4.15	3.70	0.18	0.17	9.88	5.91	0.94	0.98

[a]Figure 8 shows the location of the parts of the models averaged. The results for the resistor are for a 45 to 149 km depth range, and for the conductor they are for a 118 to 270 km depth range.

indicate the presence of macroscopic resistivity structures. The induction arrow results do not exclude the presence of resistivity anisotropy within the study area, but they do establish the presence of some large-scale resistivity structures. Thus, the conductive directions established by the GB decomposition are now taken to represent the geoelectric strike of macroscopic resistivity structures.

6. Anisotropic Two-Dimensional Inversion

The MT data for profile 1 were remodeled using 2-D anisotropic inversion. Profile 1 was chosen as the first profile for this analysis because it has the largest number of MT sites and the best coverage of the tectonic units in the northern Grenville Province. The approach was not applied to the other profiles after it was determined that there is minimal evidence for resistivity anisotropy on profile 1. *Adetunji et al.* [2014] describe 2-D isotropic modeling of this data set.

The anisotropic inversions used the 2-D anisotropic inversion code of *Mackie* [2002] and *Baba et al.* [2006]. This code fits the observed data using an anisotropic model in which the anisotropy is aligned with the structural directions, along strike (xx), across strike (yy), and vertical (zz). The code uses the nonlinear conjugate gradient method to find a solution to the 2-D inverse problem [*Mackie*, 2002]. Tikhonov regularization is implemented in terms of smoothness and anisotropy parameters. An isotropy weighting parameter (τ_{iso}) is used to control the degree of anisotropy [e.g; *Evans et al.*, 2005; *Evans et al.*, 2011; *Matsuno et al.*, 2010; *Miensopust and Jones*, 2011; *Le Pape et al.*, 2012; *Schmoldt and Jones*, 2013]. Small values of this parameter will allow for variations between the results of the diagonal of the anisotropic resistivity tensor. Values of τ_{iso} close to zero allow the models to be as anisotropic as possible, i.e., the TE and TM modes are fit independently, while the case is reversed for values of $\tau_{iso} \geq 100$ [*Mackie*, 2002].

Figure 6 compares the isotropic resistivity model for the mantle with the components of the anisotropic model produced using a smoothing regularization parameter of $\tau = 6$ and $\tau_{iso} = 1.0$, and Table 1 lists the results of the inversion. The isotropic and anisotropic models were obtained using identical grid and inversion parameters. The data error floors used in the inversions were 5% and 4% for TE and TM phases and 20% and 16% for TE and TM apparent resistivity. The isotropic model differs slightly from the one from *Adetunji et al.* [2014], and the differences are attributed to differences in the gridding and smoothing parameters between these models. The final anisotropic model produced a slightly better data fit (RMS = 2.05) than the isotropic model (RMS = 2.43). The decrease in misfit is relatively small considering the use of an anisotropy regularization factor of 1.0.

The anisotropic resistivity model for the mantle is very similar to the isotropic model; the lithospheric resistor has an identical geometry in all components of the anisotropic model. The mantle conductor at the northwest end of the model also has a similar form in all components of the anisotropic model. Figure 7 compares the resistivity on vertical cross sections through the resistor and the conductor. In general, the anisotropic model provides a smoother model than the isotropic model with lower resistivity in the resistor and higher resistivity in the upper part of the conductor. The results show minimal evidence for anisotropy in the mantle lithosphere with all three components of the resistivity model exhibiting very similar resistivity values.

The anisotropy in the resistor and in the conductor was quantified using resistivity values extracted from a region of the anisotropic model extending from 45 to 150 km depth in the resistor and from 120 to 270 km depth in the conductor (Figure 8). The resistivity values extending across each averaging volume at each available depth were combined by geometric averaging to provide a representative value for each depth.

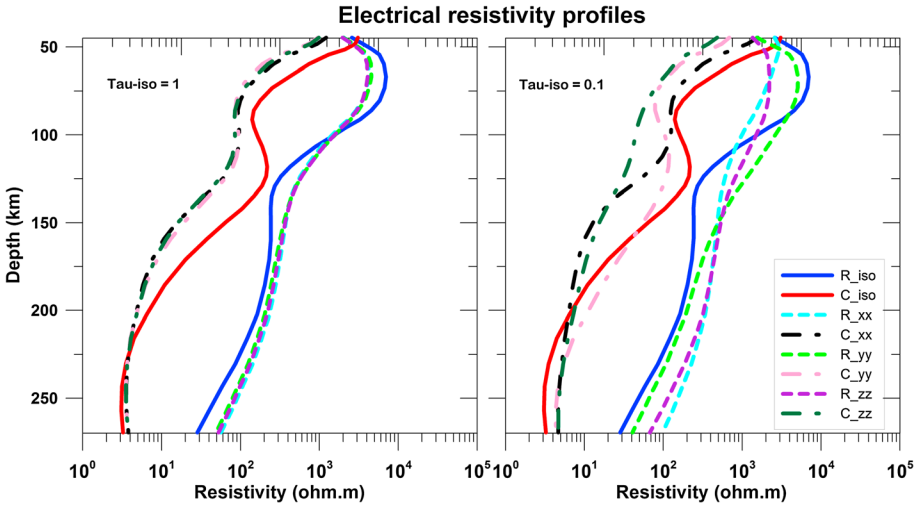

Figure 7. Resistivity profiles through the mantle resistor and mantle conductor for the isotropic and anisotropic models. Each panel compares the results from the isotropic model with the three components of resistivity from the anisotropic model: along-strike = ρ_{xx}, cross-strike = ρ_{yy}, and vertical = ρ_{zz}. (left) $\tau_{iso} = 1$ and (right) $\tau_{iso} = 0.1$. *R*_iso = profile through the resistor in the isotropic model, *C*_iso = profile through the conductor in the isotropic model.

The ratio of the across-strike to along-strike resistivity ρ_{yy}/ρ_{xx} and the ratio of the vertical to along-strike resistivity ρ_{zz}/ρ_{xx} were computed at each depth. Finally, we computed the mean and median of these ratios as representative values of the anisotropy. The results are tabulated in Table 1. Within the resistor there is an indication of very slight lateral anisotropy with higher conductivity along strike. However, the lateral anisotropy is less than about 5%. There is minimal vertical anisotropy, with the mean and median ratios for ρ_{zz}/ρ_{xx} being very close to unity.

The results provide firm confirmation that there is minimal anisotropy in the resistive upper lithosphere at, and to the immediate south of, the Grenville Front. It is of note that the $\tau_{iso} = 1.0$ anisotropic model does indicate more strongly anisotropic zones at shallower depths within conductive zones of the crust of the CMB (not shown in Figure 7). This result is in accord with *Adetunji et al*. [2014], who interpreted enhanced conductivity in these zones as being associated with graphitic rocks. Studies using the same anisotropy regularization factor of 1.0 in different tectonic settings have revealed significant anisotropy within the mantle in those locations [*Baba et al*., 2006; *Le Pape et al*., 2012]. We can therefore conclude quite reliably that there is minimal resistivity anisotropy in the resistive lithosphere. The lateral anisotropy is significantly less than 10% or approximately 2 orders of magnitude smaller than the ratio of 1:15 determined previously by *Mareschal et al*. [1995] using 1-D modeling. The results also show that there is minimal anisotropy within the lithospheric conductor where the anisotropy ratios are also less than 10% different from unity (Table 1).

To further test for the existence of anisotropy, models were obtained using even smaller isotropic regularization parameters. The resulting model for $\tau_{iso} = 0.1$ produces only a slight decrease in the misfit with an RMS misfit of 1.99 (as opposed to RMS =2.05 for $\tau_{iso} = 1$). This decrease is extremely small considering the increase in the effective number of model parameters produced by the factor of 10 decrease in the anisotropy regularization factor and provides further support for the presence of minimal mantle lithospheric anisotropy in the study area. The results indicate the presence of lateral anisotropy in both the resistor and conductor with a ρ_{yy}/ρ_{xx} ratio of about 2 and minimal vertical anisotropy. However, examination of the resistivity model shows that the major features of the model have become less spatially coherent. In particular, the resistor is subdivided into parts and the conductor includes a small internal zone of increased conductivity. For this reason the model is not considered an optimal inversion solution.

For completeness, a very rough model was also obtained with an extreme value of $\tau_{iso} = 0.01$. This model has an RMS misfit of 1.96, with minimal improvement over the $\tau_{iso} = 0.1$ model. In the rough resistivity model the mantle resistor is now divided into three parts, and within the conductor there is a focusing of the enhanced conductivity into a small zone. It is not considered a reasonable resistivity model. The anisotropy is

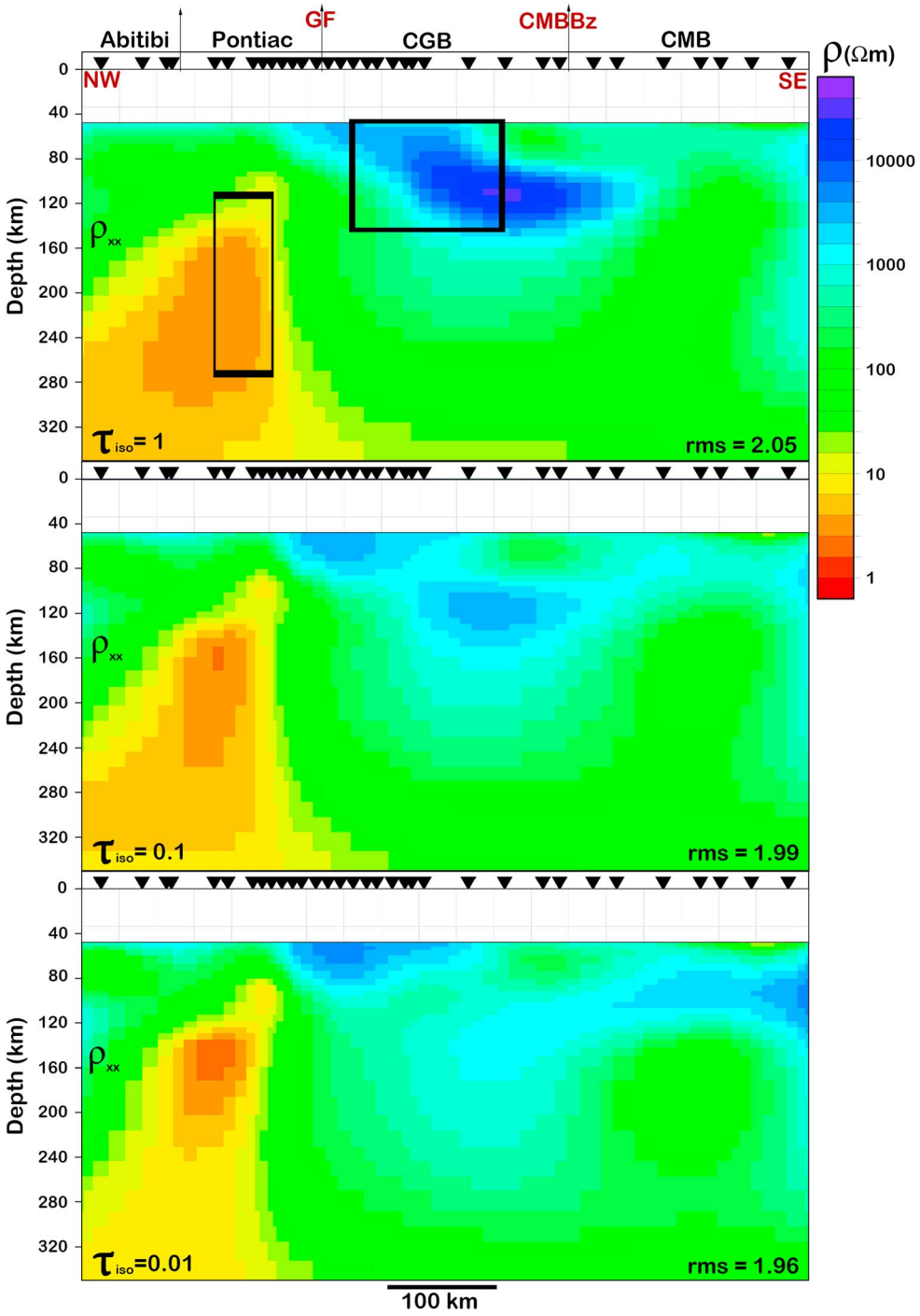

Figure 8. The along-strike component of the anisotropic inversion models for profile 1 with different value of τ_{iso}. The crustal section (upper 48 km) of the model is not shown. The rectangles show the parts of the model used to calculate the results shown in Table 1.

characterized by a maximum ρ_{yy}/ρ_{xx} ratio of about 4 in the resistor and minimal vertical anisotropy in the conductor. More significant vertical anisotropy occurs in the resistor and lateral anisotropy in the conductor. Although the corresponding resistivity model is not considered reasonable, this model allows us to completely exclude the possibility of the presence of the previously interpreted 15:1 resistivity anisotropy within the resistive mantle lithosphere.

7. Discussion and Interpretation

7.1. Geoelectric Directionality

The present study has extended earlier determinations of geoelectric dimensionality and directionality in the mantle of the study area by using a depth-based approach and by using a broader distribution of MT sites than *Adetunji et al*. [2014] and older analyses.

Within the upper lithospheric mantle depth range in areas near the Grenville Front and in the northern CGB, the conductive direction is approximately east-west. For profiles 1 and 2, the azimuth is N85°E (e.g., Figure 4). For profile 3 the direction is E20°S, but examination of GB misfit curves by *Adetunji et al*. [2015] shows that a regional N85°E azimuth is associated with only slightly higher misfit than the E20°S azimuth. The MT data are thus consistent with a common lithospheric conductive direction over a ~300 km (east-west) by 200 km (north-south) region of the northern Grenville Province. This result is in accord with the earlier analysis of *Mareschal et al*. [1995] who determined a regional azimuth of N80°E along profile 1 (Figure 1). However, the tensor decomposition applied in the present study shows that this azimuth extends significantly farther to the east than interpreted by *Mareschal et al*. [1995], to at least as far as profile 2.

The results show that the east-west azimuth observed in the upper lithosphere near the Grenville Front is very well defined in the 45–100 km and 100–150 km depth range but is more variable at depths of 150–200 km, i.e., below the resistor (Figure 4). As shown by the 2-D inversion results the conductive direction is caused by large-scale geoelectric structure rather than resistivity anisotropy ,so it can be interpreted to be associated with structures in and near the northwestern margin of the mantle lithospheric resistor.

There are two possible contributions to the observed strike azimuths. The first contribution is from internal macroscopic structures within the resistive lithosphere. The observed east-west strikes are subparallel to the Archean fabric of the Superior craton and so are consistent with this source. The second possible contribution is from the margin of the resistive block itself. For profile 1, *Adetunji et al*. [2014, 2015] interpreted this margin as being associated with refertilization related to the Mesozoic kimberlitic magmatism in the Kirkland Lake and Cobalt kimberlite fields. However, even in this case, the azimuth of the feature may reflect the original Archean fabric, as the refertilization is interpreted to have occurred through a zone of weakness in the lithosphere associated with the original formation of the Abitibi greenstone belt [e.g., *Faure et al*., 2011]. The MT results in the current study do provide support for aspects of the earlier interpretation of *Mareschal et al*. [1995] who interpreted strike directions in the southern Superior as being related to metasomatism of mantle roots of major Archean shear zones.

The mean conductive direction at $>$200 km depth in the Grenville Province is oblique to both the seismic anisotropy in the study region, as defined by the seismic shear wave (SKS) fast direction, and the GPS-based Absolute Plate Motion (APM) direction [*Adetunji et al*., 2015]. Similar obliquity has been observed in other Precambrian terrains in the world [e.g., *Simpson*, 2001; *Hamilton et al*., 2006]. Based on its obliquity to the present APM, we interpret the deeper strike direction in the Grenville to be associated with lower lithospheric structure. The lower lithosphere in the study area is interpreted to have been metasomatized by fluids associated with the Cretaceous kimberlitic magmatism. We therefore hypothesize that the observed deep MT conductive direction was established at the time of this process.

The results of the large-scale shear wave study of *Yuan et al*. [2011] indicate a depth-dependent fast axis within the lithosphere across much of North America. For locations near the present study area, the results [*Yuan et al*., 2011, Figure 8] show an approximately east-west fast direction at 70 km depth, a north-south fast direction at 150 km depth, and a southwest-northeast strike direction at 250 km depth. The MT strike direction determined for the upper lithosphere is in good agreement with the seismic fast direction in the upper lithosphere. However, the MT strike directions do not show evidence of the north-south azimuth determined by *Yuan et al*. [2011] for the lower lithosphere. This difference may relate to the localized spatial variations of the two-layer lithosphere suggested by the MT resistivity models.

7.2. Resistivity Anisotropy

The results of the present study along with the 2-D isotropic inversion results of *Adetunji et al*. [2014, 2015] indicate that the MT response anisotropy near the Grenville Front is due to large-scale geoelectrical structure rather than to resistivity anisotropy, as had previously been interpreted. The availability of induction arrows

from a broader region than in the earlier studies [e.g., *Kellett et al*., 1992] shows that at periods longer than about 30 s there is a dominant alignment of the real and imaginary arrows in a direction at high angle to the geoelectric fast direction. This observation is consistent with the presence of macroscopic resistivity structures, and the 2-D inversion models demonstrate the presence of such structures.

The 2-D anisotropic modeling in this study shows that models obtained with $\tau_{iso} = 1.0$ reveal minimum anisotropy at mantle depths. The results show that within the lithospheric resistor, the resistivity differs in the two horizontal directions by less than 6%. Other studies using the same value of the anisotropic regularization factor have revealed significant mantle resistivity anisotropy [*Baba et al*., 2006; *Le Pape et al*., 2012], and in the present study the inversions done using this factor revealed significant anisotropy at shallower depths in the CMB crust. Consideration of results obtained with lower anisotropic regularization factors indicated that in the extreme case of $\tau_{iso} = 0.01$, for which the actual resistivity models become geologically infeasible, the maximum horizontal anisotropy in the resistive lithosphere is a factor of 5, well less than the factor of 15 determined in earlier 1-D modeling studies. We conclude that there is no significant resistivity anisotropy in the upper lithospheric mantle. The results also provide no evidence for vertical anisotropy within the lithospheric conductor.

The presence of shearing in the lithosphere beneath the Grenville Front is supported by the seismic anisotropy results that show alignment of the SKS fast direction around the Grenville Front [*Sénéchal et al*., 1996; *Ji et al*., 1996; *Frederiksen et al*., 2006]. However, the new MT results show that there is no corresponding electrical anisotropy. If dextral shearing occurred, it appears to have not caused any significant shape preferred electrical anisotropy as previously interpreted. The obliquity between the seismic and MT responses is explained by the difference in azimuth of the macroscopic electrical resistivity structures in the upper lithosphere and that of the seismic anisotropy.

The present study does not exclude the presence of resistivity anisotropy farther to the north in the Superior Province [e.g., *Kellett et al*., 1992; *Kurtz et al*., 1993; *Mareschal et al*., 1995; *Ji et al*., 1996]. However, it is clear that the interpretation of resistivity anisotropy in this area should also be reassessed using modern 2-D isotropic and anisotropic inversion methods and that it is inappropriate to now base such an interpretation on 1-D inversion only.

8. Conclusions

The electrical anisotropy of the lithospheric mantle beneath the Grenville Front and the Grenville Province in Ontario, Canada, is investigated using the MT method. Data from a total of 56 sites on three profiles with northwest-southeast azimuths, spanning a north-south distance of 500 km and an east-west distance of 650 km, are analyzed. Modern depth-based tensor decomposition techniques along with anisotropic 2-D inversion are applied. The paper updates the work of *Kellett et al*. [1992, 1994], *Zhang et al*. [1995], *Mareschal et al*. [1995], *Sénéchal et al*. [1996], *Ji et al*. [1996], *Frederiksen et al*. [2006], and *Adetunji et al*. [2014, also submitted manuscript, 2015]. A major objective of this paper was to determine whether the azimuthal variation in the MT responses near the Grenville Front, defined by earlier studies, is related to electrical anisotropy or to larger-scale geological structure.

The spatially uniform MT responses noted at the Grenville Front are observed to extend to ~200 km southeast of the front and for at least 400 km along strike and are associated with very resistive lithosphere at less than 150 km depth. Farther to the southeast the geoelectric strike in the upper lithosphere has a SW-NE azimuth. The mean conductive direction at $>$200 km depth in the Grenville Province also has a SW-NE azimuth and is oblique to both the mean seismic anisotropy in the study region, as defined by the SKS fast direction, and the GPS-based APM direction.

Careful examination of the induction arrows at long periods, from an area larger than in previous studies, shows significant alignment of the real and imaginary arrows in a direction at high angle to the geoelectric strike. This observation is consistent with the presence of macroscopic resistivity structures, which is confirmed by the 2-D inversion models. The results of 2-D anisotropic modeling indicate that the mantle lithosphere beneath the Grenville Front and Grenville Province is almost electrically isotropic (i.e., anisotropy is not required to fit the 2-D lithospheric resistivity model). For anisotropic models obtained with $\tau_{iso} = 1.0$, the maximum anisotropy in both resistive and conductive regions of the lithosphere is less than 10%. This result contrasts with the factor

of 15 resistivity anisotropy determined in earlier 1-D modeling studies. We can therefore conclude that the MT response anisotropy near the Grenville Front is related to large-scale geoelectric structure rather than resistivity anisotropy, as interpreted in previous studies. A similar interpretation can be made for the observed azimuthal variation of MT responses further southeast within the Grenville Province.

We suggest that earlier interpretation of MT responses from the Grenville Front, which involves dextral shearing in the upper lithospheric mantle, should be reviewed. The obliquity between the seismic and MT responses arises because the fabric of the Archean Superior lithosphere beneath the Grenville Front is oblique to the SKS fast direction. If dextral shearing occurred, it appears to have not caused any significant shape preferred electrical anisotropy as interpreted. Our results do not exclude the existence of resistivity anisotropy to the northwest within the Superior Province, but we suggest that this possibility be reexamined with contemporary 2-D isotropic and anisotropic inversion methods.

Acknowledgments

The authors thank the POLARIS southern Ontario MT team (J. Wenham, M. Serzu, X. Ma, E. Gowan, H. Sealey, T. Pacha, B. Eade, J. McCutcheon, I. Asudeh, C. Andrews, C. Samson, and P. Fernberg) for MT data collection and landowners in the region for site access. Comments from A. Frederiksen, an anonymous reviewer, and the Associate Editor led to significant improvement of the manuscript. Some figures were produced using Wessel and Smith's GMT package. Funding for POLARIS has been provided by industry, the Canada Foundation for Innovation, provincial agencies from Ontario and British Columbia, the Federal Economic Development Initiative for Northern Ontario, Natural Resources Canada, and NSERC (Natural Sciences and Engineering Research Council of Canada). The present research was supported by an NSERC Discovery grant (105748) to Ian Ferguson.

References

Adetunji, A. Q. (2014), Resistivity structure of the Precambrian Grenville Province, Canada, PhD thesis, Dep. of Geol. Sci., Univ. of Manitoba, Winnipeg, Canada.

Adetunji, A. Q., I. J. Ferguson, and A. G. Jones (2014), Crustal and lithospheric scale structures of the Precambrian Superior-Grenville margin, *Tectonophysics*, *614*, 146–169, doi:10.1016/j.tecto.2013.12.008.

Adetunji, A. Q., I. J. Ferguson, and A. G. Jones (2015), Imaging the mantle lithosphere of the Grenville Province: Large-scale electrical resistivity structure, *Geophys. J. Int.*, doi:10.1093/gji/ggv0660, in press.

Baba, K., P. Tarits, A. D. Chave, R. L. Evans, G. Hirth, and R. L. Mackie (2006), Electrical structure beneath the northern MELT line on the East Pacific Rise at 1545'S, *Geophys. Res. Lett.*, *33*, L22301, doi:10.1029/2006GL027528.

Boerner, D. E., R. D. Kurtz, and J. A. Craven (2000), A summary of electromagnetic studies on the Abitibi-Grenville transect, *Can. J. Earth Sci.*, *37*, 427–437.

Booker, J. R. (2014), The magnetotelluric phase tensor: A critical review, *Surv. Geophys.*, *35*, 7–40, doi:10.1007/s10712-013-9234-2.

Bostick, F. X. (1977), A simple almost exact method of MT analysis, Workshop on Electrical Methods in Geothermal Exploration, *U.S. Geol. Surv.* Contract No. 14080001-8-359.

Caldwell, T. G., H. M. Bibby, and C. Brown (2004), The magnetotelluric phase tensor, *Geophys. J. Int.*, *158*, 457–469.

Carr, S. D., R. M. Easton, R. A. Jamieson, and N. G. Culshaw (2000), Geologic transect across the Grenville orogen of Ontario and New York, *Can. J. Earth Sci.*, *37*, 193–216.

Chave, A. D., and A. G. Jones (2012), *The Magnetotelluric Method—Theory and Practice*, 570 pp., Cambridge Univ. Press, Cambridge, U. K.

Crough, S. T. (1981), Mesozoic hot spot epeirogeny in eastern North America, *Geology*, *9*, 2–6.

Culshaw, N. G., A. Davidson, and L. Nadeau (1983), Structural subdivisions of the Grenville Province in the Parry Sound-Algonquin region, Ontario, in *Current Research Part B, Geol. Surv. Can. Pap. 83-1B*, pp. 243–252, Nat. Resour. Can., Ottawa, doi:10.4095/109286.

Culshaw, N. G., R. A. Jamieson, J. W. F. Ketchum, N. Wodicka, D. Corrigan, and P. H. Reynolds (1997), Transect across the northwestern Grenville orogen, Georgian Bay, Ontario: Polystage convergence and extension in the lower orogenic crust, *Tectonics*, *16*, 966–982, doi:10.1029/97TC02285.

Davidson, A. (1998), Questions of correlation across the Grenville Front east of Sudbury, Ontario, in *Current Research 1998-C*, *Geol. Surv. Can. Pap. 98-IC*, pp. 145–154, Nat. Resour. Can., Ottawa, doi:10.4095/292222.

Davidson, A., N. G. Culshaw, and L. Nadeau (1982), A tectono-metamorphic framework for part of the Grenville Province, Parry Sound region, Ontario, in *Current Research Part A, Geol. Surv. Can. Pap. 82-1A*, pp. 175–190, Nat. Resour. Can., Ottawa, doi:10.4095/119587.

Du Frane, W. L., J. J. Roberts, D. A. Toffelmier, and J. A. Tyburczy (2005), Anisotropy of electrical conductivity in dry olivine, *Geophys. Res. Lett.*, *32*, L24315, doi:10.1029/2005GL023879.

Easton, R. M. (1992), The Grenville Province and the Proterozoic history of Central and Southern Ontario, in *Geology of Ontario*, *Ontario Geol. Sur. Spec.*, vol. 4, pp. 713–904, Ontario Ministry of Northern Development and Mines, Ontario, Canada.

Eaton, D. W., et al. (2005), Geophysical arrays to investigate lithosphere and earthquake hazards in Canada, *Eos Trans. AGU*, *86*, 169–173, doi:10.1029/2005EO170001.

Eaton, D. W., S. Dineva, and R. Mereu (2006), Crustal thickness and Vp/Vs variations in the Grenville orogen (Ontario, Canada) from analysis of teleseismic receiver functions, *Tectonophysics*, *420*, 223–238.

Eisel, M., and K. Bahr (1993), Electrical anisotropy in the lower crust of British-Columbia—An interpretation of a magnetotelluric profile after tensor decomposition, *J. Geomagn. Geoelectr.*, *45*, 1115–1126.

Evans, R. L., G. Hirth, K. Baba, D. Forsyth, A. Chave, and R. Mackie (2005), Geophysical controls from the MELT area for compositional controls on oceanic plates, *Nature*, *437*, 249–252.

Evans, R. L., et al. (2011), Electrical lithosphere beneath the Kaapvaal craton, southern Africa, *J. Geophys. Res.*, *116*, B04105, doi:10.1029/2010JB007883.

Everett, M. E. (2005), What do electromagnetic induction responses measure?, *Leading Edge*, *24*, 154–157.

Faure, S., S. Godey, F. Fallara, and S. Trepanier (2011), Seismic architecture of the Archean North American mantle and its relationship to diamondiferous kimberlite fields, *Econ. Geol.*, *106*, 223–240.

Frederiksen, A. W., I. J. Ferguson, D. Eaton, S. K. Miong, and E. Gowan (2006), Mantle fabric at multiple scales across an Archean-Proterozoic boundary, Grenville Front, Canada, *Phys. Earth Planet. Int.*, *158*, 240–263.

Griffin, W. L., S. Y. O'Reilly, B. J. Doyle, N. J. Pearson, H. Coopersmith, K. Kivi, V. Malkovets, and N. Pokhilenko (2004), Lithosphere mapping beneath the North American plate, *Lithos*, *77*, 873–922.

Groom, R. W., and R. C. Bailey (1989), Decomposition of magnetotelluric impedance tensors in the presence of local three-dimensional galvanic distortion, *J. Geophys. Res.*, *94*, 1913–1925, doi:10.1029/JB094iB02p01913.

Groom, R. W., and R. C. Bailey (1991), Analytic investigations of the effects of near-surface three-dimensional glavanic scatterers on MT tensor decompositions, *Geophysics*, *56*, 496–518.

Haggart, M. J., R. A. Jemieson, P. H. Reynold, T. E. Krogh, C. Beaumont, and N. G. Culshaw (1993), Last gasp of the Grenville Orogeny: Thermochronology of the Grenville Front Tectonic Zone near Killarney, Ontario, *J. Geol.*, *101*, 575–589.

Hamilton, M. P., A. G. Jones, R. L. Evans, S. Evans, C. J. S. Fourie, X. Garcia, A. Mountford, J. E. Spratt, and the SAMTEX Team (2006), Electrical anisotropy of South African lithosphere compared with seismic anisotropy from shear-wave splitting analysis, *Phys. Earth Planet. Int.*, *158*, 226–239.

Heise, W., and J. Pous (2001), Effects of anisotropy on the two-dimensional inversion procedure, *Geophys. J. Int.*, *147*, 610–621, doi:10.1046/j.0956-540x.2001.01560.x.

Heise, W., and J. Pous (2003), Anomalous phases exceeding 90° in magnetotellurics: Anisotropic model studies and a field example, *Geophys. J. Int.*, *155*, 308–318, doi:10.1046/j.1365-246X.2003.02050.x.

Heise, W., T. G. Caldwell, H. M. Bibby, and C. Brown (2006), Anisotropy and phase splits in magnetotellurics, *Phys. Earth Planet. Int.*, *158*, 107–121.

Hirth, G., R. L. Evans, and A. D. Chave (2000), Comparison of continental and oceanic mantle electrical conductivity: Is the Archean lithosphere dry?, *Geochem. Geophys. Geosyst.*, *1*, 1030, doi:10.1029/2000GC000048.

Ji, S., S. Rondenay, M. Mareschal, and G. Senechal (1996), Obliquity between seismic and electrical anisotropies as a potentiai indicator of movement sense for ductile shear zones in the upper mantle, *Geology*, *24*, 1033–1036.

Jones, A. G. (1983), On the equivalence of the "Niblett" and "Bostick" transformations in the magnetotelluric method, *J. Geophys.*, *53*, 72–73.

Jones, A. G. (1988), Static shift of magnetotelluric data and its removal in a sedimentary basin environment, *Geophysics*, *53*, 967–978.

Jones, A. G. (1992), Electrical conductivity of the continental lower crust, in *Continental Lower Crust*, edited by D. M. Fountain et al., pp. 81–143, Elsevier, Amsterdam.

Jones, A. G. (2006), Electromagnetic interrogation of the anisotropic Earth: Looking into the Earth with polarized spectacles, *Phys. Earth Planet. Int.*, *158*, 281–291.

Jones, A. G. (2012), Distortion of magnetotelluric data: Its identification and removal, in *The Magnetotelluric Method: Theory and Practice*, edited by A. D. Chave and A. G. Jones, pp. 219–295, Cambridge Univ. Press, U. K.

Jones, A. G., and J. E. Spratt (2002), A simple method for deriving the uniform field MT responses in auroral zones, *Earth Planets Space*, *54*, 443–450.

Jones, A. G., J. Ledo, I. J. Ferguson, J. A. Craven, M. J. Unsworth, M. Chouteau, and J. E. Spratt (2014), The electrical resistivity of Canada's lithosphere and correlation with other parameters: Contributions from LITHOPROBE and other programmes, *Can. J. Earth Sci.*, *51*, 573–617, doi:10.1139/cjes-2013-0151.

Karato, S. (1990), The role of hydrogen in the electrical conductivity of the upper mantle, *Nature*, *347*, 272–273.

Kellett, R. L., M. Mareschal, and R. D. Kurtz (1992), A model of lower crustal electrical anisotropy for the Pontiac Subprovince of the Canadian Shield, *Geophys. J. Int.*, *111*, 141–150.

Kellett, R. L., A. E. Barnes, and M. Rive (1994), The deep structure of the Grenville Front: A new perspective from western Quebec, *Can. J. Earth Sci.*, *31*, 282–292.

Kurtz, R. D., E. R. Niblett, J. A. Craven, R. A. Stevens, and J. C. Macnae (1988), Electromagnetic studies over the Kapuskasing structural zone, in *Lithoprobe Kapuskasing Transect*, Lithoprobe Rep., vol. 4, pp. 167–176.

Kurtz, R. D., J. A. Craven, E. R. Niblett, and R. A. Stevens (1993), The conductivity of the crust and mantle beneath the Kapuskasing Uplift: Electrical anisotropy in the upper mantle, *Geophys. J. Int.*, *113*, 483–498.

Le Pape, F., A. G. Jones, J. Vozar, and W. Wenbo (2012), Penetration of crustal melt beyond the Kunlun Fault into northern Tibet, *Nat. Geosci.*, *5*, 330–335.

Mackie, R. L. (2002), User manual and software documentation for two-dimensional inversion of magnetotelluric data, Anisotropy Version 6.7, GSY-USA, Inc., San Francisco, Calif.

Mackwell, S., and D. Kohlstedt (1990), Diffusion of hydrogen in olivine: Implications for water in the mantle, *J. Geophys. Res.*, *95*, 5079–5088, doi:10.1029/JB095iB04p05079.

Mareschal, M., R. L. Kellett, R. D. Kurtz, J. N. Ludden, S. Ji, and R. C. Bailey (1995), Archean cratonic roots mantle shear zones and deep electrical anisotropy, *Nature (London)*, *375*, 134–137.

Martí, A. (2014), The role of electrical anisotropy in magnetotelluric responses: From modelling and dimensionality analysis to inversion and interpretation, *Surv. Geophys.*, *57*, 179–218, doi:10.1007/s10712-013-9233-3.

Matsuno, T., et al. (2010), Upper mantle electrical resistivity structure beneath the central Mariana subduction system, *Geochem. Geophys. Geosyst.*, *11*, Q09003, doi:10.1029/2010GC003101.

McNeice, G. W., and A. G. Jones (2001), Multisite, multifrequency tensor decomposition of magnetotelluric data, *Geophysics*, *56*, 158–173.

Meyer, H. O. A., M. A. Waldman, and B. L. Garwood (1994), Mantle xenoliths from kimberlite near Kirkland Lake, Ontario, *Can. Mineral.*, *32*, 295–306.

Miensopust, M. P., and A. G. Jones (2011), Artefacts of isotropic inversion applied to magnetotelluric data from an anisotropic Earth, *Geophys. J. Int.*, *187*, 677–689.

Miensopust, M. P., A. G. Jones, M. R. Muller, X. Garcia, and R. L. Evans (2011), Lithospheric structures and Precambrian terrane boundaries in northeastern Botswana revealed through magnetotelluric profiling as part of the Southern African Magnetotelluric Experiment, *J. Geophys. Res.*, *116*, B02401, doi:10.1029/2010JB007740.

Niblett, E. R., and C. Sayn-Wittgenstein (1960), Variation of electrical conductivity with depth by the magneto-telluric method, *Geophysics*, *25*, 998–1008.

Nieuwenhuis, G., M. J. Unsworth, D. Pana, and J. A. Craven (2013), Three dimensional resistivity structure of Southern Alberta, Canada: Implications for Pre-Cambrian tectonics, *Geophys. J. Int.*, *197*, 838–859.

Parkinson, W. D. (1962), The influence of continents and oceans on geomagnetic variations, *Geophys. J. R. Astron. Soc.*, *6*, 441–449.

Pek, J., and T. Verner (1997), Finite-difference modelling of magnetotelluric fields in two-dimensional anisotropic media, *Geophys. J. Int.*, *128*, 505–521, doi:10.1111/j.1365-246X.1997.tb05314.x.

Poe, B. T., C. Romano, F. Nestola, and J. R. Smyth (2010), Electrical conductivity anisotropy of dry and hydrous olivine at 8 GPa, *Phys. Earth Planet. Inter.*, *181*, 103–111.

Pommier, A. (2014), Interpretation of magnetotelluric results using laboratory measurements, *Surv. Geophys.*, *35*, 41–84.

Rasmussen, T. M. (1988), Magnetotellurics in Southwestern Sweden: Evidence for electrical anisotropy in the lower crust?, *J. Geophys. J. R. Astron. Soc.*, *89*, 799–820.

Rivers, T. (1997), Lithotectonic elements of the Grenville Province: Review and tectonic implications, *Precamb. Res.*, *86*, 117–154.

Rivers, T., J. Martignole, C. F. Gower, and A. Davidson (1989), New tectonic subdivisions of the Grenville Province, southeast Canadian Shield, *Tectonics*, *8*, 63–84, doi:10.1029/TC008i001p00063.

Rivers, T., N. Culshaw, A. Hynes, A. Indares, R. Jamieson, and J. Martignole (2012), The Grenville Orogen—A post-lithoprobe perspective, in *Tectonic Styles in Canada: The Lithoprobe Perspective*, edited by J. A. Percival et al., *Geol. Assoc. Can. Spec. Pap.*, *49*, 97–236.

Schmoldt, J.-P., and A. G. Jones (2013), A novel anisotropic inversion approach for magnetotelluric data from subsurfaces with orthogonal geoelectric strike directions, *Geophys. J. Int.*, *195*, 1576–1593.

Schock, R. N., A. G. Duba, and T. J. Shankland (1989), Electrical conduction in olivine, *J. Geophys. Res.*, *94*, 5829–5839, doi:10.1029/JB094iB05p05829.

Sénéchal, G., S. Rondenay, M. Mareschal, J. Guilbert, and G. Poupinet (1996), Seismic and electrical anisotropies in the lithosphere across the Grenville Front, Canada, *Geophys. Res. Lett.*, *23*, 2255–2258, doi:10.1029/96GL01410.

Simpson, F. (2001), Resistance to mantle flow inferred from the electromagnetic strike of the Australian upper mantle, *Nature*, *412*, 632–635.

Simpson, F., and A. Tommasi (2005), Hydrogen diffusivity and electrical anisotropy of a peridotite mantle, *Geophys. J. Int.*, *160*, 1092–1102, doi:10.1111/j.1365-246X.2005.02563.x.

Sleep, N. H. (1990), Monteregian hotspot track: A long-lived mantle plume, *J. Geophys. Res.*, *95*, 21,983–21,990, doi:10.1029/JB095iB13p21983.

Vozoff, K. (1991), The magnetotelluric method, in *Electromagnetic Methods in Applied Geophysics*, edited by M. N. Nabighian, pp. 641–711, Soc. of Explor. Geophys., Tulsa, Okla.

Wannamaker, P. E. (2005), Anisotropy versus heterogeneity in continental solid earth electromagnetic studies: Fundamental response characteristics and implications for physicochemical state, *Surv. Geophys.*, *26*, 733–765.

Weckmann, U., O. Ritter, and V. Haak (2003), A magnetotelluric study of the Damara Belt in Namibia: 2. MT phases over 90° reveal the internal structure of the Waterberg Fault/Omaruru Lineament, *Phys. Earth Planet. Int.*, *138*, 91–112.

Weidelt, P. (1999), 3D conductivity models: Implications of electrical anisotropy, in *Three-Dimensional Electromagnetics*, edited by M. Oristaglio and B. Spies, pp. 119–137, Soc. of Explor. Geophys., Tulsa, Okla.

Wessel, P., and W. H. F. Smith (1991), Free software help map and display data, *Eos Trans. AGU*, *72*, 441, doi:10.1029/90EO00319.

White, D. J., D. A. Forsyth, I. A. Asudeh, S. D. Carr, H. Wu, R. M. Easton, and R. F. Mereu (2000), A seismic-based cross-section of the Grenville Orogen in Southern Ontario and western Quebec, *Can. J. Earth Sci.*, *37*, 183–192.

Wu, X., I. J. Ferguson, and A. G. Jones (2005), Geoelectric structure of the Proterozoic Wopmay Orogen and adjacent terranes, Northwest Territories, Canada, *Can. J. Earth Sci.*, *42*, 955–981.

Yuan, H., B. Romanowicz, K. M. Fischer, and D. Abt (2011), 3-D shear wave radially and azimuthally anisotropic velocity model of the North American upper mantle, *Geophys. J. Int.*, *184*, 1237–1260, doi:10.1111/j.1365-246X.2010.04901.x.

Zhang, P., L. B. Pedersen, M. Mareschal, and M. Chouteau (1993), Channelling contribution to tipper vectors: A magnetic equivalent to electrical distortion, *Geophys. J. Int.*, *113*, 693–700.

Zhang, P., M. Chouteau, M. Mareschal, R. D. Kurtz, and C. Hubert (1995), High frequency magnetotelluric investigation of crustal structure in north-central Abitibi, Quebec, Canada, *Geophys. J. Int.*, *120*, 406–418.